A room temperature low-threshold ultraviolet plasmonic nanolaser

A Room-temperature Low-threshold Ultra-violet Plasmonic Nanolaser

Qing Zhang[1], *Guangyuan Li*[1], *Xinfeng Liu*[1], *Fang Qian*[2], *Yat Li*[3], *Tze Chien Sum*[1, 4], *Charles M. Lieber*[5,*], *Qihua Xiong*[1,6,*]

[1]Division of Physics and Applied Physics, School of Physical and Mathematical Sciences, Nanyang Technological University, Singapore 637371

[2]Physical and Life Sciences Directorate, Lawrence Livermore National Laboratory, Livermore, California 94550, United States

[3]Department of Chemistry and Biochemistry, University of California, Santa Cruz, California 95064, United States

[4]Singapore-Berkeley Research Initiative for Sustainable Energy, 1 Create Way, Singapore 138602, Singapore

[5]Department of Chemistry and Chemical Biology, Harvard University, Cambridge, Massachusetts 02138, United States

[6]NOVITAS, Nanoelectronics Centre of Excellence, School of Electrical and Electronic Engineering, Nanyang Technological University, Singapore, 639798

*To whom correspondence should be addressed. Email address: Qihua@ntu.edu.sg; cml@cmliris.harvard.edu.

Constrained by large ohmic and radiation losses, plasmonic nanolasers operated at visible regime are usually achieved either with a high threshold (10^2-10^4 MW/cm^2) or at cryogenic temperatures (4-120 K). Particularly, the bending-back effect of surface plasmon (SP) dispersion at high energy makes the SP lasing below 450 nm more challenging. Here we demonstrate the first strong room-temperature ultra-violet (UV, ~370 nm) surface plasmon polariton laser with an extremely-low-threshold (~3.5 MW/cm^2). We find that a closed-contact planar semiconductor-insulator-metal interface greatly lessens the scattering loss, and more importantly, efficiently promotes the exciton-SP energy transfer thus furnishes adequate optical gain to compensate the loss. An excitation polarization-dependent lasing action is observed and interpreted with a microscopic energy transfer process from excitons to SPs. Our work advances the fundamental understanding of hybrid plasmonic waveguide laser and provides a solution of realizing room-temperature UV nanolasers for biological applications and information technologies.

Introduction

Conventional laser medium has a size limit to the half of the optical wavelength in the dielectric medium. Surface plasmon (SP) provides a solution to break this diffraction limit through storing optical energy into free electron collective oscillations.[1-3] Surface plasmon nanolaser has recently attracted considerable interest due to its unprecedented capability of generating intense coherent light sources in the deep sub-wavelength regime, offering strong light-matter interaction and many advanced applications in nanophotonics and information technology[4, 5]. The lasing of surface plasmon, including localized surface plasmon (LSP) and propagating surface plasmon polariton (SPP), has been demonstrated in metal nanosphere cavities[6], metal-cladding nanoresonators[7, 8], insulator/metal nanowaveguides[9-14], and coupled plasmonic crystal[15-19]. The plasmonic cavities exhibit ultra-small modal volume V_m ~ 1/10-1/1000, enabling the tailoring of the strong light-matter interaction in a variety of linear ($\sim Q/V_m$) and nonlinear ($\sim Q^2/V_m$ or $Q/V_m^{1/2}$) optical process, where Q is the cavity quality factor. However, due to high intrinsic metal ohmic losses and radiation leakage, particularly in visible and ultra-violet regime, the Q ranges ~ 10-100 which is still much smaller than their dielectric counterpart[20-23]. As a result, the threshold of optical-pumped visible plasmonic lasing (400 -700 nm) is still nearly three-order higher than II-VI/III-VI semiconductor nanostructure photonic lasing. At such an intense excitation condition, cryogenic operation is widely adopted to promote optical gain and prevent device damages[7, 9, 12], which considerably limits the practical applications. Till now, it is still a big challenge to realize low-threshold room-temperature surface plasmon laser.

Ultra-violet (UV) laser (200–400 nm) holds important applications from high-resolution bio-imaging, drug detection, laser therapy to optical storage[24-27]. However, as the optical wavelength approaches to the inter/intra-band transition energy (*e.g.* ~ 326 nm for Ag), the intrinsic ohmic loss increases dramatically thus decreases the SP propagating length[4, 28]. For instance, to sustain a plasmonic lasing at 400 nm along SiO_2/Ag film, an optical gain of ~ 10^5 cm^{-1} is needed[4]. Moreover, the rapidly-increased damping loss limits a high energy asymptote in the SPP dispersion (*i.e.* at ~ 360 nm for SiO_2-Ag film), so-called bending-back effect[29], principally discouraging the SP lasing action above the energy limit. Hence so far, there remains an obstacle

of surface plasmon lasing below 450 nm. Recent effort on UV nanolasers particularly using metal-cladded GaN stripes or nanorods has been reported, however the deep-subwavelength mode volume is still challenging due to a small photonic-SP modal overlap or un-prohibited photonic mode[30-32]. The hybrid plasmonic waveguide laser device, through confining electromagnetic energy into a deep sub-wavelength insulator layer with propagating SPP, exhibits particular important applications in quantum information and biophotonics for straightforward propagating route, low dissipation loss and relatively high *Q*-factor[4, 6, 33-35].

Here we report an intense, single-mode, room-temperature optically pumped UV SPP nanolaser. The SPP lasing (~370 nm) threshold is ~3.5 MW/cm^2, which is almost 1000-times lower than that was reported in other room-temperature visible plasmonic nanolaser. We demonstrate that the outstanding performance of the plasmonic laser device is attributed to high nanowire crystalline quality and a closed-contact planar semiconductor-insulator-metal interface, which can support efficient exciton-plasmon energy transfer, large regions of high Purcell factor and low scattering loss. Moreover, we prove a dominating exciton to surface plasmon energy channel via the evidence of incidence polarization sensitive lasing action, revealing the concept of SPP lasing in the hybrid plasmonic waveguide nanolaser devices.

Results

Structure of low-loss ultra-violet plasmoinc laser devices

In such nanolaser device, three factors are critical to realize a SP lasing in UV region: high-quality cavity, well-defined contact interface, effective photonic and plasmonic modal coupling. Figure 1a schematically shows the device structure consisting of a triangular GaN nanowire sitting on an aluminum (Al) film separated with a thin layer of silica (SiO_2). Al is adopted as the plasmonic medium due to its smaller ohmic loss in the UV regime compared to silver[24]. The gain coefficient of GaN nanowires is expected as large as ~10,000 cm^{-1} (Ref.13, Ref. 36). To reduce the interface scattering loss, the evaporation condition of Al and SiO_2 film is optimized to obtain a flat and continuous surface with a root mean square surface roughness below 0.5 nm (Supplementary Figure 1)[13]. Particularly, the GaN nanowire exhibits a triangular cross section, which constructs a fully planar semiconductor-insulator-metal interface. The edge and interface scattering loss within

the planar interface is significantly suppressed, compared with a point interface in cylindrical nanowire-dielectric-metal structures[9, 13]. Moreover, the large contact area ensures a larger photonic-plasmonic modal overlap and implements an effective energy-transfer channel of exciton-plasmon coupling (see details in Discussion), to make full use of the optical gain from semiconductor.

Figure 1b shows the simulated cross-sectional electric field distribution of the GaN-SiO_2-Al structure (λ~370 nm, Method). The GaN nanowire edge length a is ~100 nm. The electromagnetic energy is concentrated in the thin 8-nm-insulator gap region, exhibiting a deep-subwavelength modal volume of ~$\lambda^2/68$ (Methods). On the other hand, the confinement factor in the GaN nanowire is ~3.42, indicating that a high percentage of the bulk material gain supplied by the GaN nanowire is harnessed in this hybrid configuration. The local Purcell factor distribution inside the GaN nanowires is displayed in Fig. 1c, suggesting that most of the GaN nanowire regime exhibits a pronounced Purcell factor of ~7-10, supporting the effective coupling between the semiconductor waveguide and the SPP mode.

Lasing characterization of plasmonic device

The plasmonic laser device (Fig. 2a) is optically pumped by a 355 nm nanosecond-pulsed laser (Methods). The incident polarization is made to be circular to eliminate the emission polarization response to excitation, and the emission light along and perpendicular to nanowire long axis (c) is collected individually (Fig. 2b). Below the lasing threshold (I_{ex} ~0.5 MW/cm^2), pronounced Fabry-Pérot oscillations (arrows, Fig. 2c) can be resolved over a broad band-edge emission band of GaN nanowires (370 nm, room temperature), suggesting the observation of the longitudinal cavity modes resonated between two nanowire end facets. The emission intensity along the nanowire axis (red curve, Fig. 2c) is stronger than the perpendicular component (blue curve, Fig. 2c), manifesting the dominate waveguiding of SPP in the cavity. A high group refractive index n_g of 7.61 is extracted out using the linear relationship between $\delta\lambda \sim 1/L$ (Figure 2c, inset), which agrees well with our calculation (n_g~8.96, Method). The group index can be further increased with the pumping fluence and decreasing of the nanowire diameter due to a higher carrier density, stronger coupling and larger loss[9, 10].

With I_{ex}=2.5−4.0 MW/cm^2, the output power shows a super-linear increase, with an appearance of a sharp peak (FHMW ~ 0.8 nm) over the spontaneous emission background, suggesting the occurrence of amplified spontaneous emission (Fig. 2d). As I_{ex} is further increased beyond 4 MW/cm^2, the spectrum is concentrated and dominant with the sharp peak (full lasing action). The integrated emission intensity including the spontaneous background I_{out} on a log-log scale suggests a threshold of 3.5 MW/cm^2 (Fig. 2b, inset). The lasing threshold value is in good agreement with a theoretical prediction based on loss-compensation model in hybrid plasmonic waveguide laser[37]. Moreover, the lasing threshold is three orders of magnitude lower than that of the other room-temperature plasmonic nanolaser device (~ GW/cm^2) (Ref. 12).

Numerical analysis of plasmonic and photonic mode

How to validate the surface plasmon lasing is an important issue[18, 19, 38]. In this work, mode simulation, emission polarization properties and time-resolved spectroscopy are conducted to prove the observation of plasmonic lasing. Calculations on the GaN nanowire edge length (a) dependence of the effective index and field distribution for the hybrid plasmonic and photonic modes are performed. The effective index n_{eff} used to quantify the phase velocity in the direction along nanowire axis is proportional to the real part of the eigenvalue β, *i.e.* $n_{eff} = Re\{\beta\} / k_0$, where k_0 is the incident wave vector. In GaN-SiO_2 configuration (photonic device, Fig. 3a), photonic modes such as HE11-like, EH11-like, TE01-like and TM01-like modes are supported if a > ~ 220 nm (Fig. 3c). The electric field distribution can be seen in Supplementary Figure 2a [39]. If when a < ~130 nm, all the four photonic modes are prohibited, as indicated by the vertical dashed line in Figure 3c.

In GaN-SiO_2-Al configuration (plasmonic device, Fig. 3b), the typical hybrid mode distributions indicate that not only the hybrid plasmonic mode but also the hybrid photonic modes can be supported (see Supplementary Figure 2b). However, the hybrid photonic modes, supported in the GaN-SiO_2-Al configuration due to a large permittivity mismatch, are cut-off as a < ~110 nm (Fig. 3d). Only one hybrid plasmonic mode exists if a is between 50 nm and ~110 nm, which suggests that the lasing action observed in Fig. 2d is due to the hybrid plasmonic mode. We notice in Fig. 3c that no photonic mode can be supported in GaN nanowire when a < ~130 nm, however

it is still possible to support hybrid photonic modes EH11-1 when the nanowire is sitting on SiO_2-Al structure (Fig. 3d). As a result, it is more precise to determine the cut-off size for photonic mode in the semiconductor-insulator-metal configuration instead of in the semiconductor-SiO_2 configuration as done previously[9].

Emission polarization of plasmonic and photonic lasing

The longitudinal plasmonic and photonic modes exhibit distinct polarization behavior[9, 33]. Figure 4a and 4b present the simulated near-field (left) and far-field (right) polarization distributions (**E**-field) of the emission scattered out from the nanowire tips. In the plasmonic device (GaN-SiO_2-Al), the electric field normal to the metal surface exhibits the strongest coupling to SPP, thus the emission is highly polarized along the nanowire axis (Fig. 4a). However, in photonic device (GaN-SiO_2), the transverse electric modes waveguide and oscillate inside the GaN nanowires, leading to a stronger emission with the polarization perpendicular to the nanowire axis (Fig. 4b). Experimentally, as shown by Fig. 4c, the plasmonic lasing is significantly polarized along the nanowire; while in photonic lasing mode the perpendicular component is stronger than the parallel component (Supplementary Figure 3). The polarization of plasmonic lasing, influenced by incidence polarization (discussion later) and collection angle *etc*, is ~ 50% for $\mathbf{E}_{out}//c$ which is comparable with previous works[13, 14]. The polarization dependence of the spontaneous emission below the threshold is also observed, taken along the GaN nanowire across the Al boundary (Fig. 4d). The nanowire on top of SiO_2-Al exhibits a dominating $\mathbf{E}_{out}//c$ emission, while the nanowire directly sitting on SiO_2 substrate shows a dominating $\mathbf{E}_{out}\perp c$ emission, suggesting that it is not the dielectric distinction or exciton transition but the plasmonic cavity determining the polarization[40]. To conclude, the dominating $\mathbf{E}_{out}//c$ emission in plasmonic mode, supported by the cut-off size prediction discussed previously, unambiguously confirm the achievement of plasmonic lasing.

Purcell Effect

The spontaneous emission decay rate of GaN nanowire is significantly enhanced in the plasmonic device due to Purcell effect[41-43]. As shown in Fig. 4e, the GaN emission lifetime, measured by a two-photon excitation (Methods), decreases from 698 (photonic device) to 78 ps (plasmonic device). The Purcell factor of ~ 8.9 corresponds to a mode that is a hundred times

smaller than the diffraction limit, which agrees with our analytical calculations (Fig. 1b) and local Purcell factor distribution (Fig. 1c).

More interestingly, we find that the SPP lasing modes are sensitive to incident polarization. In the previous reports on plasmonic nanolasers, the incident polarization has not been considered[9, 12, 13]. Instead of using a circularly polarized laser, we use linearly polarized laser to pump the same nanowire, and to detect the lasing emission from the tip in two polarizations (Fig. 5a). When the incident polarization is along the nanowire ($\mathbf{E}_{in}//c$), the plasmonic lasing exhibits a single-mode operation centered at 369 nm, with a higher intensity along the nanowire axis (Fig. 5b). If the incident polarization is rotated by 90^0 ($\mathbf{E}_{in}\perp c$), multi-mode emission appears with the strongest mode red shifted to 372 nm (Fig. 5c), nevertheless the polarization is still dominated by $\mathbf{E}_{out}//c$ emission. However, the lasing intensity and the polarizing ratio is larger when the incident polarization is along the nanowire, indicating a more effective hybridization or a stronger coupling between the semiconductor waveguide and the SPPs. The larger modal overlap results in a better cavity quality and therefore single mode lasing is obtained.

Incidence polarization-sensitive plasmonic lasing

The polarization-sensitive lasing behavior can be well-understood by combining the passive hybrid plasmonic waveguide approach with a microscopic active photon-exciton-SPP interaction model. Based on the quantum theory of plasmonic lasing[4, 18, 44], the tremendous SPP transition energy to achieve population inversion in metal system is furnished by gain media via nonradiative energy transfer from excitons to surface plasmon. Therefore, the population and coupling efficiency of exciton to the SPP mode are important to plasmonic lasing performance (*Q*-factor and threshold, *etc*). The total electric field distribution excited by the incident pump at 355 nm, which determines the population and distribution of launched excitons, is calculated to evaluate the population and coupling efficiency. Figure 5d shows the *z*-component when the incident polarization is along the *c*-axis, in which both the *x*- and *y*-components are zero. Figure 5e and f display the E_x (5e) and E_y (5f) components of the total excitation electric field when the incident polarization is perpendicular to *c*-axis (355 nm), in which the *z*-component is zero. The dipoles in the GaN nanowire embodying the gain are assumed to be polarized parallel to the total electric field. Figures 5g-i show the local dipole-field coupling efficiency[45] inside the GaN

nanowire into hybrid plasmonic mode as a function of the position of the dipole for each polarization. Only the *y*- and *z*-polarized dipoles can couple to the hybrid plasmonic modes therefore will drive plasmonic lasing. The effective gain harvested by the hybrid plasmonic mode is then determined by multiplying the dipole population, which is proportional to the total excitation electric field intensity $|\mathbf{E}|^2$ in the nanowire gain region, and the local dipole-field coupling efficiency. By integrating the effective gain inside the GaN nanowire the total effective gain for $\mathbf{E}_{in}//c$ is estimated to be ~ 1.87 times over that for $\mathbf{E}_{in}\perp c$ (details in Supplementary Figure 4 and Supplementary Discussion), which agrees well with the corresponding ratio of measured peak emission intensity in Figs. 5b and c (about 1.46). In other words, the relatively larger effective gain harvested leads to a stronger lasing intensity when the pump polarization is along nanowire axis.

Although there are experimental observations of lasing based on the hybrid plasmon waveguide devices, the claim of the surface plasmon lasing is still very controversial[38, 46]. A fundamentally important issue, *i.e.*, whether the lasing nature is an amplification of stimulated surface plasmon emission or only a plasmon-assisted photonic lasing, has to be clarified. SPP lasing is accomplished by efficient energy transfer from exciton to SPP. However, in plasmon-assisted photonic lasing an inverse energy transfer process is dominated, which is usually manifested as enhanced luminescence and more rapid radiative decay channels due to strong localized electromagnetic field. Our experiments of excitation-polarization sensitive lasing behaviors suggest that the energy is transferred from exciton to SPP in hybrid plasmonic devices.

Discussion

To achieve plasmonic lasing, the modal loss α_m must be overcompensated by the modal gain g_m, such as $g_m > \alpha_m$ (Refs 47&48). The loss in a plasmonic cavity α_m is mainly contributed by four parts: intrinsic ohmic damping ($\alpha_{e\text{-}scat}$, $\alpha_{e\text{-}h}$) and extrinsic radiation (γ_{rad}) and scattering losses (γ_{scat}). $\alpha_{e\text{-}scat}$ and $\alpha_{e\text{-}h}$ is the absorption coefficient of individual free-electron scattering (with electrons, lattice ions, impurities, *etc*) and the inter/intra-band transition for excitation of electron-hole pairs, respectively (Fig. 6a)[28]; γ_{rad} and γ_{scat} is the radiation and scattering loss in the plasmonic cavities respectively (Fig. 6b)[9, 13]. The intrinsic ohmic loss is mainly determined by metal itself,

while the extrinsic loss can be effectively reduced via clever design of the plasmonic cavities (symmetry, roughness, and facet reflectance, etc). In principle, γ_{rad} occurs primarily at the nanowire end (Fig. 6b, I) which can be evaluated as $-2/L \times \ln R$, where R is the facet reflectance of SPP mode. To reduce the γ_{rad}, long nanowire (L=15 μm) is adopted. On the contrary, the total intrinsic ohmic loss is much larger than γ_{rad} by nearly one order of magnitude (Method). To further improve the Q values, smart design of high reflective plasmonic cavity is demanded, such as using distributed Brag reflector structure. Secondly, γ_{scat} arises via scattering of propagating surface plasmon to localized surface plasmon or out of plasmonic cavity (Fig. 6b. II), which occurs mainly at rough semiconductor-insulator-metal interface[47]. In our work, the root mean square surface roughness of SiO_2-Al and Al film is optimized down to sub-nanometers (0.454 nm and 0.359 nm, respectively) to minimize γ_{scat}. Furthermore, the construction of a planar interface using triangular nanowires relatively decreases the edge scattering ratio, which even holds a stronger confinement of electromagnetic wave inside the cavity (Fig. 6b, III).

Another important issue is how to harness optical gain from active media thoroughly. The plasmonic lasing process can be facilitated by three steps: an exciton in gain media is launched by the incident photons; then the excitons recombine nonradiatively and the energy is transferred to metal system via excitation of a surface plasmon; the surface plasmon stimulates the excitons in gain media to create more surface plasmons. During the second and third steps, a high efficiency of non-radiative energy transfer between exciton and SP is critical to achieving population inversion of SP. The SP population variation can be expressed as

$$dN_{sp} = N_{ex}.R_{ex\text{-}SP}.n_{eff}/c dz, \qquad \text{(eq.1)}$$

where N_{ex} is the exciton population, $R_{ex\text{-}SP}$ is the exciton-SP non-radiative energy transition rate, t, z are surface plasmon propagating time and distance respectively, and c is the light speed in free-space. From the eq.1, the surface plasmon mode gain is proportional to $R_{ex\text{-}SP}$, which decays rapidly with the exciton- surface plasmon distance. Based on a dipole-dipole interaction model[49],

$$R_{ex\text{-}SP} \approx A/d^6, \qquad \text{(eq.2)}$$

A is a constant for a given system, d is the distance between SP and exciton. As d > 10 nm, the exciton-surface plasmon energy transfer efficiency is too low to provide sufficient gain to overcompensate the surface plasmon propagating loss[50]. However as d < 5 nm, the opening of

other non-radiative channels, such as electron transfer, lower the gain of active media. The speculated optimal thickness for plasmonic amplification ranges between 5 ~ 10 nm, *e.g.*, the SiO_2 insulator thickness of 8 nm deposited in this work. Furthermore, for a fixed insulator layer thickness, we believe the effective gain compensation area of a planar interface larger than cylindrical interface (shown in Fig. 6c). Therefore, we believe that the low-threshold and high-*Q* plasmonic lasing with such a short-wavelength output mode is mainly attributed to the close-contact planar interface.

Methods

Metal-insulator film deposition and characterization

To reduce the radiation loss and ensure a good contact between GaN nanowire and planar plasmonic cavity, SiO_2 on Al film with small roughness is prepared. The Al film with a thickness of 100 nm was deposited onto a 300 nm SiO_2/Si substrate by an electron-beam evaporator. The film root mean square surface roughness is ~ 0.359 nm measured by atomic force microscopy (AFM). The Al film is well-protected in vacuum and then an insulator SiO_2 layer is deposited on to the Al film by magnetron sputtering. The total root mean square surface roughness of SiO_2-Al film was measured to be ~ 0.454 nm. The SiO_2 thickness is designed to be 8 nm to form a continuous film.

Nanowire synthesis and characterization

The GaN nanowire was grown by metal-organic chemical vapor deposition (MOCVD) on sapphire substrates using trimethylgallium and ammonia as Ga and N precursors, respectively, and hydrogen as a carrier gas. The previous transmission electron microscopy (TEM) and scanning electron microscopy (SEM) studies show that the nanowire has triangular cross section and smooth surface. The nanowire edge length is 100-300 nm. The smooth surface is advantage for good contact between GaN with SiO_2-Al film. The as-grown GaN nanowires were ultrasonically removed from substrate, dispersed into isopropyl alcohol and deposited onto pre-prepared SiO_2-Al films substrate.

Optical characterizations

The plasmonic lasing measurement was conducted using a Horiba-JY T64000 spectrometer. A quasi-continuous wave laser (pulsed width: 10 ns, repetition rate: 100 KHz) with a wavelength of 355 nm is focused by an objective (40×, numerical aperture: 0.4), and the spot diameter is around 25 μm. The large laser spot ensures that the whole GaN nanowires are efficiently pumped. A quarter-wave plate is used to change the linear polarized laser source to be circularly polarized. The emission from the plasmonic devices is collected by the same objective with the back-scattering configuration and analyzed by the spectrometer. A polarization analyzer is placed before spectrometer entrance to select the emission polarization. For low-temperature lasing spectroscopy, a liquid N_2 continuous-flow microscopy cryostat was used and the samples were pasted to the cold

finger of the cryostat with silver paste to ensure good thermal conduction.

The PL and time-resolved PL spectra of an individual plasmonic device were investigated using a home-built confocal microscope system. Both the excitation pulses and emission light was coupled and collected through a 20× microscope objective (N.A. = 0.45). The pump pulses (650 nm) were generated from an optical parametric amplifier (Light Conversion TOPAS) that was pumped by a 1-kHz regenerative amplifier (Coherent Legend; center wavelength: 800 nm; pulse width: 150 fs; power: 1 mJ per pulse), which was in turn seeded by an 80 MHz Coherent Vitesse oscillator. The emission signal was collected by a spectrometer (Acton, Spectra Pro 2500i) equipped with a charge couple device camera (Princeton Instruments, Pixis 400B) (for PL measurement) or an Optronis Optoscope streak camera system (for TRPL measurement). The streak camera system has an ultimate temporal resolution of ~ 10 ps when operated at the shortest time window of 330 ps.

Numerical calculations on modal eigenvalues, loss and area

The cross-section waveguide mode properties (effective indices and field distributions) of the GaN-SiO_2-Al configuration and the configurations of GaN nanowire sitting on SiO_2 substrate were calculated using finite element method (COMSOL). The refractive indexes of GaN and SiO_2 are 2.65 and 1.46 at λ = 370 nm, respectively. The eigenvalue solver was used to find modes. Full 3D simulations using the above hybrid plasmonic mode or photonic mode as the input were performed to calculate the near-field electric field distribution and the far-field emission. Perfectly matched layers were used to mimic the open boundary conditions. In photonic mode simulation, the thickness of SiO_2 film is assumed to be infinite.

After we obtained the eigenvalues of the hybrid waveguide mode, the modal loss can be evaluated using the propagation length defined as the length a mode travels before decaying to e^{-1} of its original power, such that $\Lambda = 1/2\,\mathrm{Im}\{\beta\}$ .The modal area $A_m = \int\int_{-\infty}^{\infty} W(\mathbf{r})\,\mathrm{d}^2\mathbf{r} \Big/ \max\{W(\mathbf{r})\}$ is defined as the ratio of the total mode energy and its peak energy density, ,where $W(\mathbf{r}) = \frac{1}{2}\left[\mathrm{Re}\{\mathrm{d}(\varepsilon(\mathbf{r})\omega)/\mathrm{d}\omega\}|E(\mathbf{r})|^2 + \mu_0|H(\mathbf{r})|^2\right]$ is the energy density per unit length along the direction of propagation. $|E(\mathbf{r})|^2$ and $|H(\mathbf{r})|^2$ are the modal

electric and magnetic field distributions, respectively; $\varepsilon(\boldsymbol{r})$ is the material electric permittivity, μ_0 is the vacuum magnetic permeability. For dielectric materials (SiO_2), the material electric permittivity dispersion is disregarded, *i.e.* $d\left(\varepsilon(\mathbf{r})\omega\right)/\mathrm{d}\omega \approx \varepsilon(\mathbf{r})$; whereas, $d\left(\varepsilon(\mathbf{r})\omega\right)/\mathrm{d}\omega = \varepsilon(\mathbf{r}) + \omega\, d\varepsilon\left(\mathbf{r}\right)/\mathrm{d}\omega$ for Al. Particularly, to compensate big metal loss in the plasmonic device, high carrier density and gain threshold will pull up the dispersion of the semiconductor, therefore for GaN electric permittivity dispersion is considered, *i.e.* $d\left(\varepsilon(\mathbf{r})\omega\right)/\mathrm{d}\omega = \varepsilon(\mathbf{r}) + \omega\, d\varepsilon\left(\mathbf{r}\right)/\mathrm{d}\omega$. The above-defined mode area is a widely used figure of merit since it is inversely proportional to the spontaneous emission rate enhancement, or the Purcell factor, F_p, of an atom placed at the mode's peak energy density.

Numerical calculations on local Purcell factor

To study the local enhancement of the exciton recombination rate due to a broad-band Purcell effect, we calculated the local Purcell factor following the procedure reported previously.[9] The emission rate for a dipole emitter at position **r** within the GaN nanowire is split into components corresponding to the enhancement of the emission rate of radiation modes, F_{R}, SPP modes, F_{SPP}, and the lossy surface waves (LSW), F_{LSW}. Assuming that only a small modification of the radiative emission rate occurs, we have $F_{\mathrm{R}} \approx 1$. The SPP contribution to the Purcell factor is averaged over both of the available dipole orientations, $F_{\mathrm{spp}} = \frac{1}{2}(F_{\mathrm{SPP},x}(\mathbf{r}) + F_{\mathrm{SPP},y}(\mathbf{r}))$, where $F_{\mathrm{SPP},\mu}(\mathbf{r}) = 3n_{\mathrm{g}}\left(\lambda/2n_0\right)^2 \Big/ \pi\, n_{\mathrm{s}} A_{\mathrm{SPP},\mu}(\mathbf{r})$ is the SPP enhanced emission rate Purcell factor with an orientation along the μ direction, n_{g} is the SPP group velocity, n_{s} is the refractive index of semiconductor GaN, and $A_{\mathrm{SPP},\mu}(\mathbf{r}) = \int\int_{-\infty}^{\infty} W(\mathbf{r})\mathrm{d}^2\mathbf{r} \Big/ n_{\mathrm{s}}^2\varepsilon_0 \left|E_{\mathrm{SPP},\mu}(\mathbf{r})\right|^2$ is a measure of the mode area for a given dipole orientation and position. Lossy surface waves are associated with high in-plane momentum leaky waves of the metal and are extremely localized, $F_{\mathrm{LSW}} = \left(\varepsilon_{\mathrm{m}}''\varepsilon_{\mathrm{s}} \Big/ 4\left|\varepsilon_{\mathrm{m}} + \varepsilon_{\mathrm{s}}\right|^2\right)\left(1\Big/\left(\mathrm{n}_{\mathrm{s}}k_0h\right)^3 + 1\Big/\left(\mathrm{n}_{\mathrm{s}}k_0h\right)\right) + \varepsilon''/16\ \mathrm{n}_{\mathrm{s}}k_0h$, where $\varepsilon_{\mathrm{m}}'' = \mathrm{Im}\left\{\varepsilon_{\mathrm{m}}\right\}$, ε_{m} and ε_{s} are the permittivity of metal Al and semiconductor GaN, respectively, h is the insulator SiO_2 gap height.

Confinement factor and lasing threshold

To achieve lasing, the threshold condition requires the modal gain per unit length should be greater than the modal loss per unit length and the average reflection loss per unit length. The bulk GaN gain threshold should be $g_0^{\mathrm{s}} > \left(\Gamma_{\mathrm{m}}\alpha_0^{\mathrm{m}} - 2/L\ln R\right)/\Gamma_{\mathrm{s}}$. $\Gamma_{\mathrm{s}} = 2n_{\mathrm{g}}W_e^s/n_{\mathrm{s}}W$,[47, 48] where

$W_e^s = \frac{1}{2}\iint_s \mathrm{Re}\left[d(\omega\varepsilon)/d\omega|\mathbf{E}|^2\right]\mathrm{d}x\mathrm{d}y$,

$W = \frac{1}{2}\iint_\infty \mathrm{Re}\left[d(\omega\varepsilon)/d\omega|\mathbf{E}|^2 + \mu_0|\mathbf{H}|^2\right]\mathrm{d}x\mathrm{d}y$

$\overline{v}_{\mathrm{g}} = \frac{1}{2}\iint_\infty \mathrm{Re}(\mathbf{E}\times\mathbf{H})\square\mathbf{z}\mathrm{d}x\mathrm{d}y \Big/ \frac{1}{2}\iint_\infty \mathrm{Re}\left[d(\omega\varepsilon)/d\omega|\mathbf{E}|^2 + \mu_0|\mathbf{H}|^2\right]\mathrm{d}x\mathrm{d}y$.

$\Gamma_{\mathrm{m}} = c\varepsilon_0 n_{\mathrm{m}}\iint_{\mathrm{m}}|\mathbf{E}|^2\mathrm{d}x\mathrm{d}y \Big/ \iint_\infty \mathrm{Re}(\mathbf{E}\times\mathbf{H})\square\mathbf{z}\mathrm{d}x\mathrm{d}y$ are the confinement factors of the semiconductor GaN nanowire and the metal region, respectively, g_0^{s} is the bulk material gain coefficient of semiconductor GaN, $\alpha_0^{\mathrm{m}} = \omega\varepsilon_{\mathrm{m}}''/(cn_{\mathrm{m}})$ is the bulk material absorption coefficient of metal with n_{m} being its real part of the refractive index, *L* is the length of the nanowire, and *R* is the modal reflection efficiency by the end facet. The gain and absorption coefficients are in unit of inverse length. As a result, Since α_0^{m} has been obtained from the data of Johnson & Christy, *L* has been readily measured, and *R* has been calculated using 3D finite element method (FEM) simulation, the key to calculate the lasing threshold lies in the confinement factor.

For the structure with GaN nanowire edge length of 100 nm, at λ = 370 nm, $\alpha_0^{\mathrm{m}} = 1.517\times10^6\ \mathrm{cm}^{-1}$, Λ = 0.58 μm, $\Gamma_{\mathrm{s}} = 3.4240$, $\Gamma_{\mathrm{m}} = 0.011$, R = 0.15, $n_{\mathrm{g}} = c/\overline{v}_{\mathrm{g}} = cW/S_z = 8.96$. The measured nanowire length *L*=15 μm, and accordingly $-2/L\ln R = 2.529\times10^3\,\mathrm{cm}^{-1}$. Then we obtained the bulk GaN gain threshold, $g_0^{\mathrm{s}} = 5778\ \mathrm{cm}^{-1}$, which is smaller than the expected gain of GaN nanowire from literature.

Acknowledgement

This work was mainly supported by Singapore Ministry of Education via an AcRF Tier2 grant (MOE2011-T2-2-051). In addition, the author Q.X. also gratefully thanks the strong support from Singapore National Research Foundation through a Fellowship grant (NRF-RF2009-06) and a Competitive Research Program (NRF-CRP-6-2010-2), and support from Nanyang Technological University via start-up grant (M58110061) and New Initiative Fund (M58110100). Q.X. thanks

Nanyang Nanofabrication Center for the help in e-beam evaporation. C.M.L. acknowledges support from a National Security Science and Engineering Faculty Fellow (NSSEFF) award from the Department of Defense. Y.L. thanks the financial support from United States NSF (DMR-0847786). T.C.S acknowledges the financial support NTU start-up grant M4080514, SPMS collaborative Research Award M4080536 and the Singapore-Berkeley Research Initiative for Sustainable Energy (SinBeRISE) CREATE Programme.

Author contributions

Q.Z. and Q.X. design the experiment. Q.Z. conducts the steady-state lasing measurement. G.Y.L performs the theoretical modeling and numerical simulation. X.F. L and T.S. conduct the two-photon pumped lifetime measurement. F. Q, Y. L and C. M. L grow the nanowires. All the authors co-wrote the manuscript.

Additional information:
Competing financial interest: No competing financial interest

Reference

1. Schuller, J. A.*et al.* Plasmonics for extreme light concentration and manipulation. *Nat Mater* **9**, 193-204 (2010).
2. Gramotnev, D. K., Bozhevolnyi S. I. Plasmonics beyond the diffraction limit. *Nat Photon* **4**, 83-91 (2010).
3. Tame, M. S.*et al.* Quantum plasmonics. *Nat Phys* **9**, 329-340 (2013).
4. Berini, P., De Leon I. Surface plasmon-polariton amplifiers and lasers. *Nat Photon* **6**, 16-24 (2012).
5. Hill, M. T. Status and prospects for metallic and plasmonic nano-lasers [Invited]. *Journal of the Optical Society of America B* **27**, B36-B44 (2010).
6. Noginov, M. A.*et al.* Demonstration of a spaser-based nanolaser. *Nature* **460**, 1110-1112 (2009).
7. Nezhad, M. P.*et al.* Room-temperature subwavelength metallo-dielectric lasers. *Nat Photon* **4**, 395-399 (2010).
8. Ding, K.*et al.* Electrical injection, continuous wave operation of subwavelength-metallic-cavity lasers at 260 K. *Applied Physics Letters* **98**, - (2011).
9. Oulton, R. F.*et al.* Plasmon lasers at deep subwavelength scale. *Nature* **461**, 629-632 (2009).
10. Hill, M. T.*et al.* Lasing in metal-insulator-metal sub-wavelength plasmonic waveguides. *Optics Express* **17**, 11107-11112 (2009).
11. Flynn, R. A.*et al.* A room-temperature semiconductor spaser operating near 1.5 ?m. *Optics Express* **19**, 8954-8961 (2011).
12. Ma, R. M.*et al.* Room-temperature sub-diffraction-limited plasmon laser by total internal reflection. *Nat Mater* **10**, 110-113 (2011).
13. Lu, Y. J.*et al.* Plasmonic Nanolaser Using Epitaxially Grown Silver Film. *Science* **337**, 450-453 (2012).
14. Wu, C. Y.*et al.* Plasmonic Green Nanolaser Based on a Metal–Oxide–Semiconductor Structure. *Nano Letters* **11**, 4256-4260 (2011).
15. Tredicucci, A.*et al.* Single-mode surface-plasmon laser. *Applied Physics Letters* **76**, 2164-2166 (2000).
16. Lakhani, A. M., Kim M. K., Lau E. K., Wu M. C. Plasmonic crystal defect nanolaser. *Optics Express* **19**, 18237-18245 (2011).
17. Marell, M. J. H.*et al.* Plasmonic distributed feedback lasers at telecommunications wavelengths. *Optics Express* **19**, 15109-15118 (2011).
18. Zhou, W.*et al.* Lasing action in strongly coupled plasmonic nanocavity arrays. *Nat Nano* **8**, 506-511 (2013).
19. van Beijnum, F.*et al.* Surface Plasmon Lasing Observed in Metal Hole Arrays. *Physical Review Letters* **110**, 206802 (2013).
20. Vahala, K. J. Optical microcavities. *Nature* **424**, 839-846 (2003).
21. Qian, F.*et al.* Multi-quantum-well nanowire heterostructures for wavelength-controlled lasers. *Nat Mater* **7**, 701-706 (2008).
22. Liu, X., Zhang Q., Xiong Q., Sum T. C. Tailoring the Lasing Modes in Semiconductor Nanowire Cavities Using Intrinsic Self-Absorption. *Nano Letters* **13**, 1080-1085 (2013).
23. Zhang, Q.*et al.* Highly Enhanced Exciton Recombination Rate by Strong Electron–Phonon Coupling in Single ZnTe Nanobelt. *Nano Letters* 12, 6420-6427 (2012).
24. Huang, M. H.*et al.* Room-Temperature Ultraviolet Nanowire Nanolasers. *Science* **292**, 1897-1899 (2001).
25. Krutmann, J., Morita A. Mechanisms of Ultraviolet (UV) B and UVA Phototherapy. *J Investig Dermatol* **4**, 70-72 (1999).
26. Johnson, J. C.*et al.* Single gallium nitride nanowire lasers. *Nat Mater* **1**, 106-110 (2002).
27. Elliott, D. J. *Ultraviolet laser technology and applications* (Academic Press, New York, 1995).
28. Johnson, P. B., Christy R. W. Optical Constants of the Noble Metals. *Physical Review B* **6**, 4370-4379 (1972).
29. Arakawa, E. T., Williams M. W., Hamm R. N., Ritchie R. H. Effect of Damping on Surface Plasmon Dispersion. *Phys. Rev. Lett.* **31**, 1127-1129 (1973).
30. Wang, Y. G.*et al.* Room temperature lasing with high group index in metal-coated GaN nanoring. *Applied Physics Letters* **99**, 251111 (2011).
31. Wang, Y. G.*et al.* Lasing in metal-coated GaN nanostripe at room temperature. *Applied Physics*

Letters **98**, 131110 (2011).
32. Hsu, Y. C.*et al.* Room temperature ultraviolet GaN metal-coated nanorod laser. *Applied Physics Letters* **103**, 191102 (2013).
33. Oulton, R. F.*et al.* A hybrid plasmonic waveguide for subwavelength confinement and long-range propagation. *Nat. Photonics* **2**, 496 (2007).
34. Gather, M. C., Meerholz K., Danz N., Leosson K. Net optical gain in a plasmonic waveguide embedded in a fluorescent polymer. *Nat Photon* **4**, 457-461 (2010).
35. Ma, R. M.*et al.* Multiplexed and Electrically Modulated Plasmon Laser Circuit. *Nano Letters* (2012).
36. Shaklee, K. L., Nahory R. E., Leheny R. F. Optical gain in semiconductors. *Journal of Luminescence* **7**, 284-309 (1973).
37. Khurgin, J. B., Sun G. Practicality of compensating the loss in the plasmonic waveguides using semiconductor gain medium. *Applied Physics Letters* **100**, - (2012).
38. Gather, M. C. A rocky road to plasmonic lasers. *Nat Photon* **6**, 708-708 (2012).
39. Ma, Y.*et al.* Semiconductor nanowire lasers. *Advances in Optics and Photonics* **5**, 216-273 (2013).
40. Wang, J.*et al.* Highly Polarized Photoluminescence and Photodetection from Single Indium Phosphide Nanowires. *Science* **293**, 1455-1457 (2001).
41. Purcell, E. *Phys. Rev.* **69**, 681 (1946).
42. Khurgin, J. B., Sun G. Injection pumped single mode surface plasmon generators: threshold, linewidth, and coherence. *Optics Express* **20**, 15309-15325 (2012).
43. Khurgin Jacob, B., Sun G. How small can “Nano” be in a “Nanolaser”? *Nanophotonics* **1**, 3-8 (2012).
44. Bergman, D. J., Stockman M. I. Surface Plasmon Amplification by Stimulated Emission of Radiation: Quantum Generation of Coherent Surface Plasmons in Nanosystems. *Physical Review Letters* **90**, 027402 (2003).
45. Sauvan, C., Hugonin J. P., Maksymov I. S., Lalanne P. Theory of the Spontaneous Optical Emission of Nanosize Photonic and Plasmon Resonators. *Physical Review Letters* **110**, 237401 (2013).
46. Ma, R. M., Oulton R. F., Sorger V. J., Zhang X. Plasmon lasers: coherent light source at molecular scales. *Laser & Photonics Reviews* **7**, 1-21 (2013).
47. Robinson, J. T., Preston K., Painter O., Lipson M. First-principle derivation of gain in high-index-contrast waveguides. *Opt. Express* **16**, 16659-16669 (2008).
48. Li, D. B., Ning C. Z. Peculiar features of confinement factors in a metal-semiconductor waveguide. *Applied Physics Letters* **96**, 181109-181103 (2010).
49. Govorov, A. O., Lee J., Kotov N. A. Theory of plasmon-enhanced Förster energy transfer in optically excited semiconductor and metal nanoparticles. *Physical Review B* **76**, 125308 (2007).
50. Peng, B.*et al.* Fluorophore-Doped Core–Multishell Spherical Plasmonic Nanocavities: Resonant Energy Transfer toward a Loss Compensation. *ACS Nano* **6**, 6250-6259 (2012).

Figures and Captions

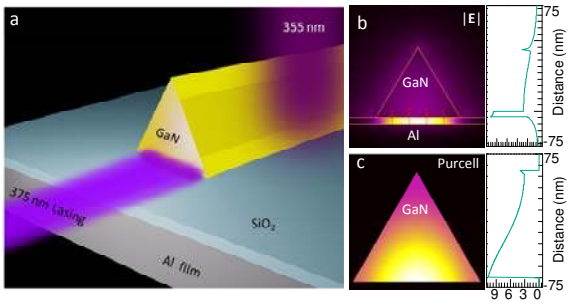

Figure 1. Ultra-violet Plasmonic Nanolaser Device. (a) Schematic of semiconductor/dielectric/plasmonic devices. GaN nanowires with a triangular cross section is supported on Al film with 8 nm SiO_2 insulator separation layer. A focused quasi-continuous wave 355 nm ultra-violet laser source is used to pump the whole GaN nanowires. The GaN photoluminescence waveguides along the high-refractive nanowire, hybridize with surface Plasmon polariton mode of Al film to produce plasmon lasing. (b) Absolute electric-field ($|E|$) distribution (left) around the plasmonic device with a wavelength of λ = 370 nm, corresponding to the lasing wavelength of GaN nanowires, calculated by a finite-element-method. The electric field direction is indicated by red arrows. The $|E|$ cross section plot (right) confirms that the optical energy is confined into the insulating SiO_2 layer with a volume confinement factor of ~ $\lambda^2/68$. (c) Calculated local Purcell factor distribution around the GaN nanowire (left) and cross-sectional Purcell factor plots (right). Large regime inside the nanowire exhibits a Purcell factor of ~7-10.

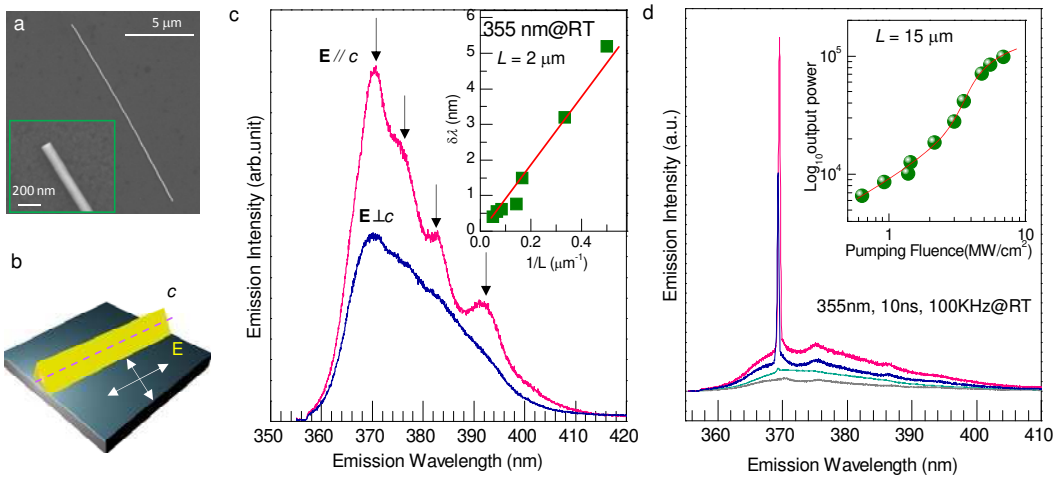

Figure 2: Room-temperature ultra-violet plasmonic lasing characterization. (a) SEM image of a GaN nanowire sitting on SiO_2/Al film. Inset: magnified scanning electron microscopy image of one end of the GaN nanowire. The nanowire length and diameter is 15 μm and 100 nm, respectively. (b) Schematic of optical measurement and polarization detection setup. *c* is defined as the orientation of nanowire. The incidence excitation laser is circular-polarized and the focused laser beam can cover the whole nanowire. The emission scattered out from two ends is collected and the polarization property along and perpendicular to nanowire axis *c* is analyzed. (c) Spontaneous emission of as-fabricated plasmonic device below lasing threshold at room-temperature under a power fluence of 0.5 MW/cm^2. Arrows highlight the Fabry-Pérot peaks. The nanowire length is 2 μm. Inset: Cavity mode spacing $\delta\lambda$ variation with nanowire length *L* (green dots). $\delta\lambda$ versus 1/*L* can be well fitted with a linear function (red curve), suggesting a high group index n_g ($n_g = \lambda^2/2L$) of 7.61 due to the high gain requirement of the plasmonic laser device. (d) Power-dependent emission spectra of the plasmonic devices. One sharp peak with a maximum FWHM ~ 0.8 nm appears above the spontaneous emission background. The nanowire length is 15 μm. Inset: integrated emission versus pumping intensity. The *S* shaped plot suggests the evolution from a spontaneous emission, amplified spontaneous emission to lasing process.

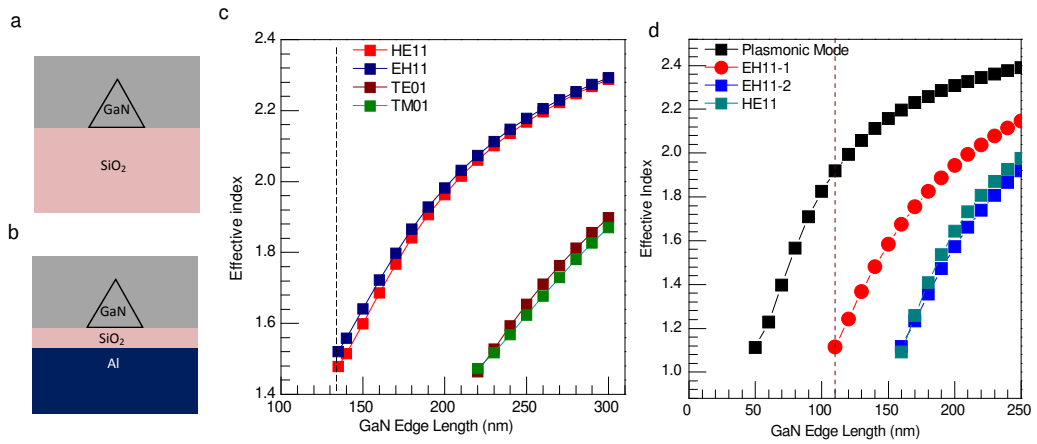

Figure 3. Modes in photonic and plasmonic devices. (a-b) Simulation configuration of photonic (a) and plasmonic devices (b). Photonic device: the GaN nanowire is sitting on a SiO_2 substrate with infinite thickness; plasmonic device: the GaN nanowire is sitting on Al substrate with a thin SiO_2 (8 nm) spacer layer. (c) The effective refractive index of HE11-like (red), EH11-like (blue), TE01-like (wine) and TM01-like (Oliver) mode versus the GaN nanowire edge length *a*. The cut-off sizes of HE11-like and EH11-like mode are around *a* = 135 nm (dashed line). (d) The effective indexes of hybrid plasmon mode (black), photonic EH11-1-like (red), EH11-2-like (green), HE-11-like (blue) modes versus the GaN nanowire edge length in plasmonic device. The cut-off size of EH11-1-like mode is around *a* = 110 nm (dashed line).

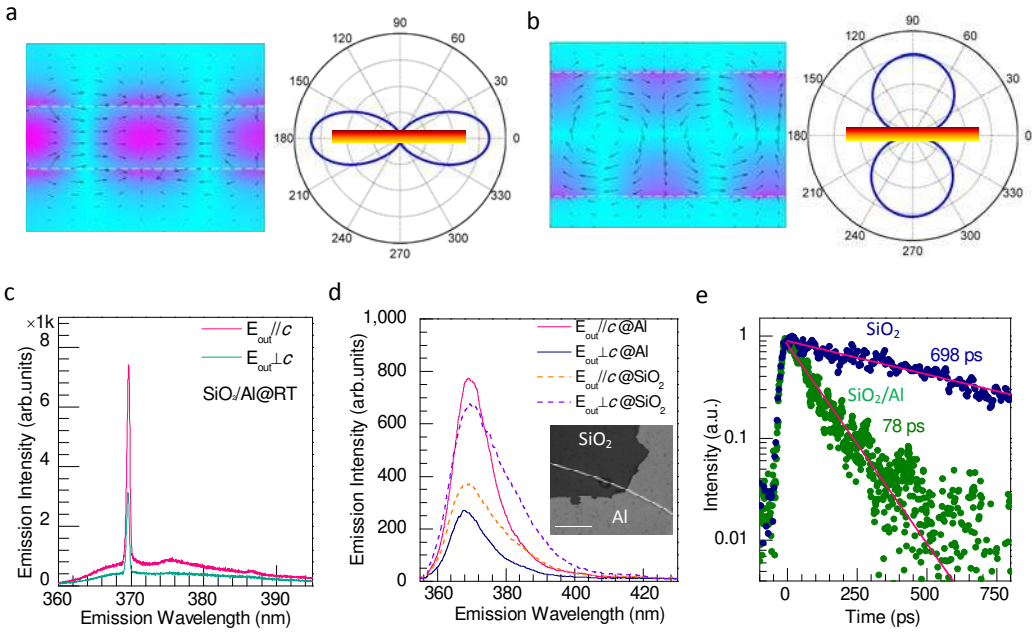

Figure 4. Plasmonic lasing polarization and Purcell effect. (a-b) Hybrid plasmonic mode polarization distribution along the thin GaN nanowire (150 nm) sitting on SiO_2/Al film (a), and photonic waveguide mode polarization distribution along thick GaN nanowires (200 nm) on SiO_2 substrate (b). Left panels: near-field electric field and oscillation direction. Black arrows indicate the electric field direction. Dashed line indicates the nanowire edge. Right panels: far-field emission intensity as a function of polarization angle. The polarization angle is defined as the angle between electric field direction and nanowire axis *c*. (c) Plasmonic lasing intensity along two polarization directions. (d) Polarization-dependent spontaneous emission spectra of the same GaN nanowire sitting on SiO_2/Al (solid curves) and SiO_2 (dashed curves) substrate along the two polarization directions. Inset: SEM image of the GaN nanowire. (e) Time-resolved two-photon pumped emission of the GaN nanowire (d) sitting on SiO_2/Al (green dots) and SiO_2 (blue dots). The decay curves can be well fitted by a single-exponential function with a lifetime of 78 and 698 ps for plasmonic and photonic device, respectively.

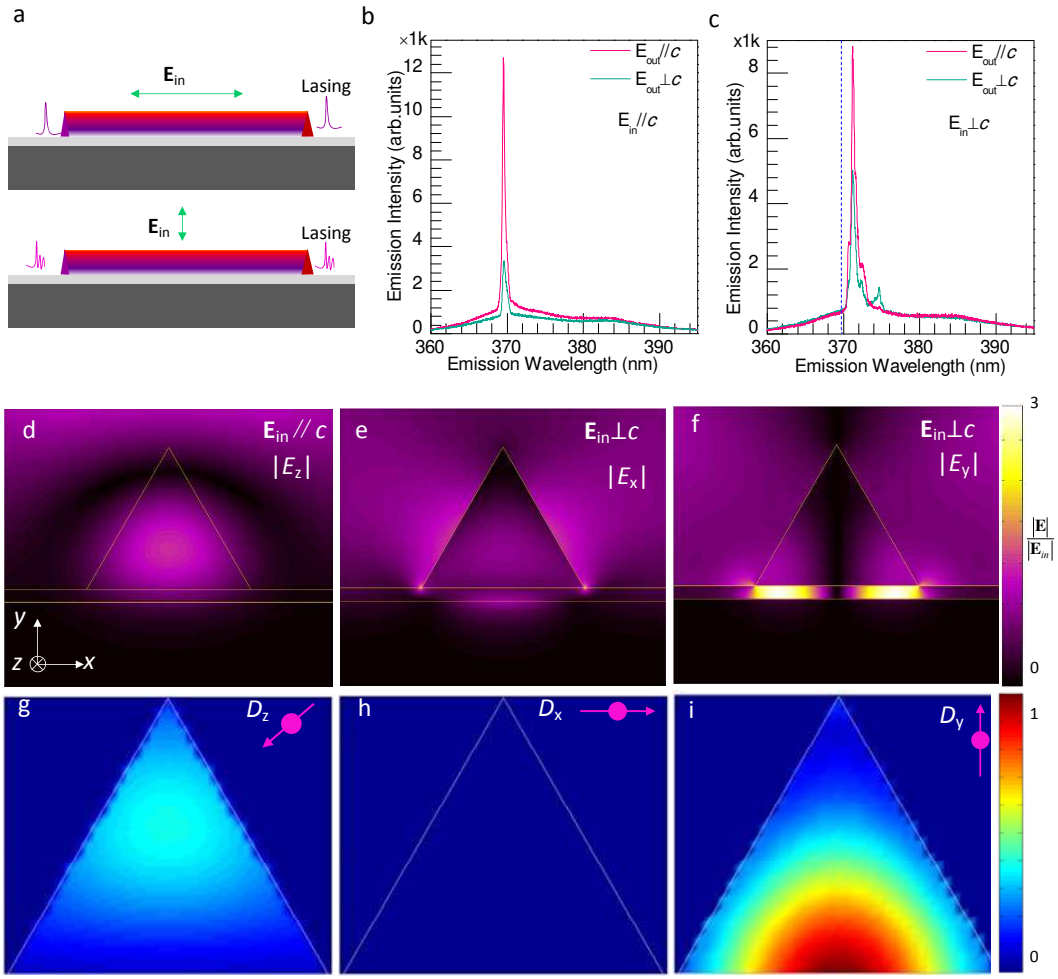

Figure 5. Incident polarization selected plasmonic lasing modes. (a) Schematic of plasmonic lasing selected by incidence polarization. Linear polarization, along (upper panel) and perpendicular to (bottom panel) the nanowire axis *c* is used to excite the plasmonic device. Single-mode (upper panel) and multi-mode (bottom panel) plasmonic lasing can be obtained respectively. (b-c) Experimental spectra when the excitation polarization is along (b) and perpendicular to (c) nanowire axis *c*. The red and green curves show the emission spectra along and perpendicular to the nanowire axis *c* respectively. (d-f) The total incident electric field in hybrid plasmonic devices as the incident polarization is along the nanowire axis *c* ($|E_z|$, d) and perpendicular to nanowire axis *c* (e: $|E_x|$; f: $|E_y|$) (g-i) The dipole-field coupling efficiency distribution of GaN exciton dipole fields into hybrid plasmonic modes along the GaN-SiO_2-Al interface. The exciton dipoles are polarized along z, *x*, *y* direction ($|E_z|$, g; $|E_x|$, h; $|E_y|$, i) .

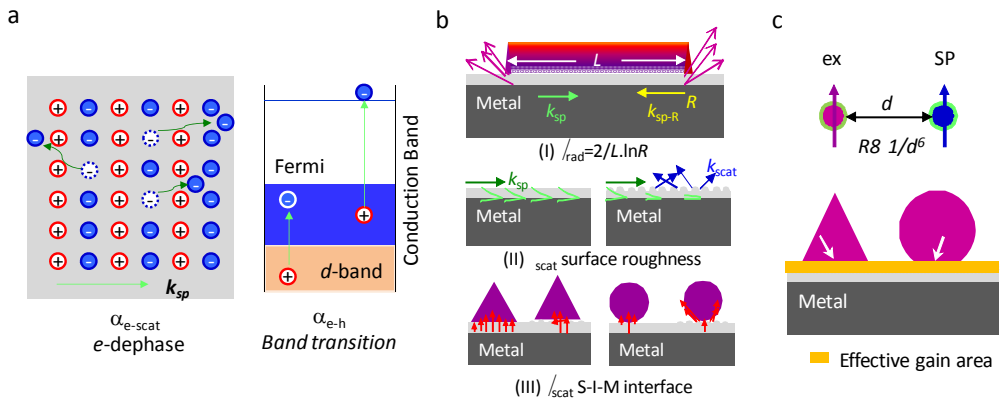

Figure 6. Loss and gain in hybrid plasmonic laser device. (a) Schematic of two surface plasmon intrinsic damping (ohmic loss) channels: nonradiative dephasing of individual electron via scattering with electrons, phonons, lattice ions and impurities at low energy, etc; excitation of electron-hole pair via intra- and inter-band transition at high energy. (b) Schematic of extrinsic surface plasmon damping via radiative emission at cavity facet (γ_{rad}, I), scattering at rough metal surface (γ_{scat}, II) and scattering at semiconductor-insulator-metal interface (III). Higher confinement and lower scattering loss is shown for a planar semiconductor-insulator-metal interface. (c) Exciton-surface plasmon energy transfer based on a dipole-dipole interaction model (upper panel). The energy transfer rate is proportional to the sixth power of the distance between them. Bottom panel: The effective gain area (yellow area), in two types of semiconductor-insulator-metal interface. The planar interface exhibits a larger effective area to supply optical gain to compensate the loss in metal.

Supplementary Figure

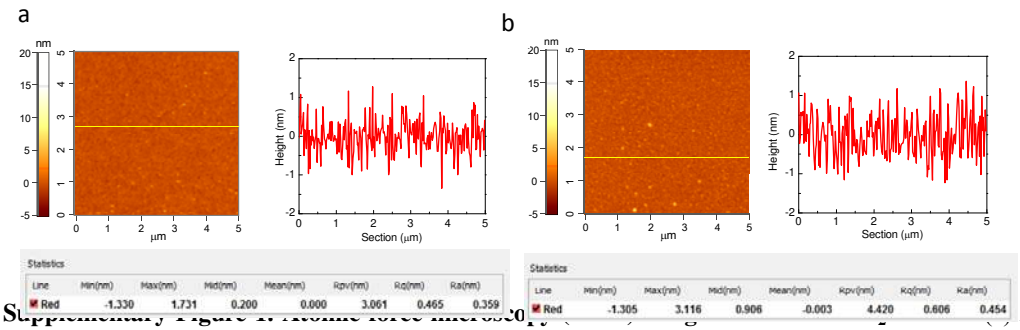

Supplementary Figure 1. Atomic force microscopy (AFM) images of (a) Al film; (b) SiO_2/Al film. Left panel is the original AFM image. Right panel is height cross section along the yellow line in left panel. The bottom panel gives the statistical data of surface roughness.

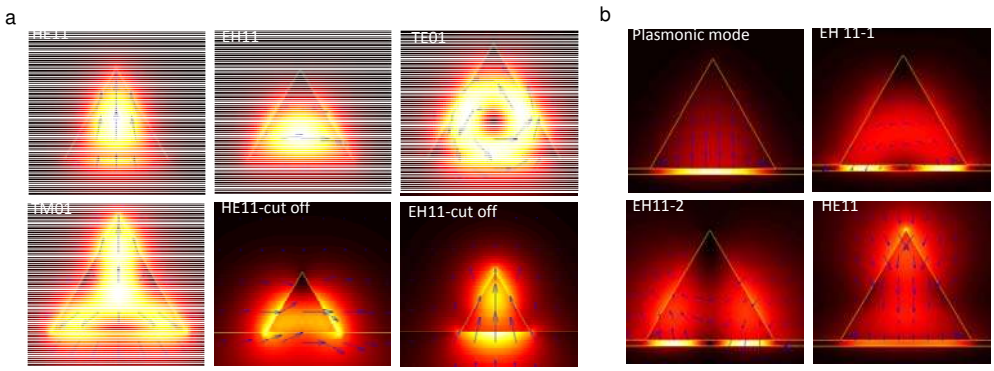

Supplementary Figure 2. Photonic mode vs. Hybrid photonic/plasmonic modes. a. Panels from left to right are the electric field distribution $|\boldsymbol{E}(x, y)|$ of HE11-like and EH11-like photonic modes in GaN-SiO_2 configuration for a = 210 nm, TE01-like and TM01-like modes for a = 270 nm, and EH11-like/TM01-like modes around cut-off size, respectively. b. The electric field distributions $|\boldsymbol{E}(x,y)|$ of four typical hybrid modes in GaN-SiO_2-Al configuration for the GaN nanowire edge length of 180 nm. The calculated propagation lengths for the four modes are 0.85, 1.26, 0.84 and 1.49 μm, respectively, and the respective normalized mode areas A_m / A_0 with $A_0 = (\lambda/2)^2$ are 0.10, 0.22, 0.22 and 0.25.

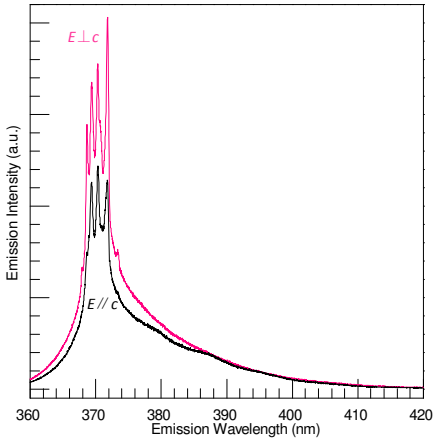

Supplementary Figure 3. Lasing in photonic laser device. The emission of a single GaN sitting on SiO_2/Si substrate as a function as pumping fluence is measured. The GaN nanowire has an edge length of 250 nm. The intensity when the lasing polarization is perpendicular to the nanowire axis c is higher than the component with a polarization along c (nanowire long axis).

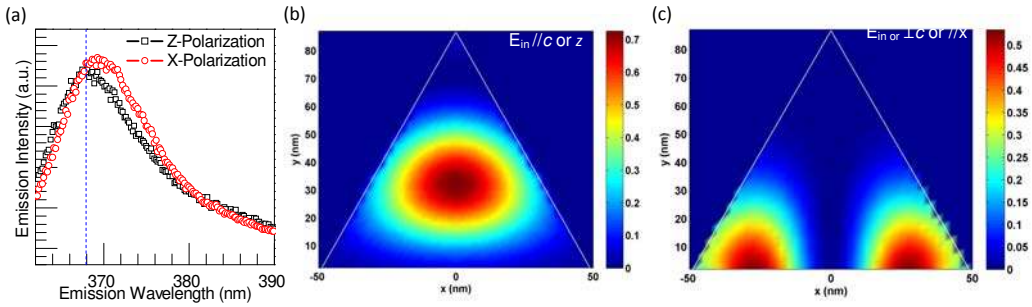

Supplementary Figure 4. (a) The PL emission of GaN nanowire below lasing threshold. The center wavelength of emission peak when the polarization is along *z* and *x* is 368 and 372 nm, respectively. The emission peak position may be due to the two types of excitons with different polarization direction in GaN nanowires. (b-c) Effective gain distribution (in arbitrary unit) in the GaN nanowire pumped by laser at 355 nm polarized perpendicular (b) or parallel (c) to the nanowire axis.

Supplementary Discussion

The dipole-field coupling efficiency:

We consider a single linearly polarized dipole emitter located at (x, y) in the GaN nanowire region, $\mathbf{p}(x,y) = p(x,y)\mathbf{u}$, with **u** = **x**, **y**, or **z** being a unit vector. The dipole emitter drives the hybrid plasmonic modes that propagate along +z and -z direction. The dipole-field coupling efficiency $A_u(x,y)$ is defined as the ratio of the total energy of the launched hybrid plasmonic fields in both directions over the energy of the dipole in bulk semiconductor. It is calculated by the overlap integral between the electromagnetic field radiated by the dipole and that of the hybrid plasmonic mode.

Since there are only nontrivial y and z components for the hybrid plasmonic mode, only dipoles polarized along y or z direction could drive the hybrid plasmonic mode. Note that the distributions and intensities of dipole-field coupling efficiency for y-polarized and z-polarized dipoles are similar to those of the E_y and E_z components of the hybrid plasmonic mode, respectively. This is due to the fact that the larger electric field of the waveguide eigenmode at the position of the single dipole emitter, the larger energy transfer from the dipole to the waveguide field. In other words, the dipole-field coupling efficiency assembles the hybrid plasmonic mode because of sampling effect. These characteristics can be understood by the following equation[8]:

$$\Gamma = \frac{2}{\hbar}\mathrm{Im}[\mathbf{p}^{*}\cdot\mathbf{E}(\mathbf{r}_0)] \qquad \text{(S12)}$$

where Γ is the spontaneous decay rate of the dipole, **E** is the total electric field that satisfies Maxwell equations in the presence of the dipole, which can be expanded into the hybrid plasmonic mode and other radiation components. We should also note that the maximum dipole-field coupling efficiency is larger than 1.0 because of the plasmon enhancement.

The effective gain

It is widely accepted that the stimulated emission rate (and thus the gain) depends on the intensity of the excitation field, which is proportional to $|\mathbf{E}|^2$. Here we further assume that the polarization of the dipoles is also parallel to the excitation electric field. As a result, for the pump laser polarized along z direction, the dipoles in the GaN region are expressed as

$$p_z(x,y) \propto |E_z|^2 \qquad \text{(S13)}$$

where E_z is the nonzero z component of the total excitation field, as shown in Fig. 5d; for the pump laser polarized along x direction, the dipoles in the GaN region are expressed as

$$p_x(x,y) \propto |E_x|^2 \,,\quad p_y(x,y) \propto |E_y|^2 \qquad \text{(S14)}$$

where E_x and E_y are nonzero x and y components of the total excitation field, as shown in Fig. 5e and f, respectively;

The effective gain harvested by the hybrid plasmonic mode is then expressed as

$$G_{eff} \propto A_z \mid E_z \mid^2 \tag{S15}$$

for the pump laser polarized along *z* direction, and

$$G_{eff} \propto A_x \mid E_x \mid^2 + A_y \mid E_y \mid^2 \tag{S16}$$

for the pump laser polarized along *x* direction.

The total effective gain is then obtained by integrating over the whole GaN nanowire region. The ratio of total effective gain in (b) over that in (c) is about 1.87, indicating the pump laser polarized parallel to the nanowire axis will result in higher lasing intensity than that polarized perpendicular to the nanowire axis, as shown in Supplementary Figure S5. The calculation result agrees well with the measured result shown in Fig. 5b and c, where the ratio of peak emission intensity for $E_{in} \| c$ over that for $E_{in} \perp c$ is about 1.46.